IUBAT Review—A Multidisciplinary Academic Journal, 8(2): 176-191
https://doi.org/10.3329/iubatr.v8i2.86886

Design of a Wide-angle Polarization Insensitive Square Ring Hybrid Resonator for Satellite Communication System

Murad Kabir Nipun[1*], F. A. Sabbir Ahmed[2], Md Golam Morshed[3], S. M. Rifatur Rana[3]

[1]*Department of Electrical and Electronic Engineering, IUBAT – International University of Business Agriculture and Technology, Dhaka, Bangladesh*

[2]*Department of Physics, IUBAT – International University of Business Agriculture and Technology*

[3]*Department of Computer Science and Engineering, IUBAT – International University of Business Agriculture and Technology*

Keywords:

Metamaterial Absorber; Polarization-Independent; Wideband Absorption; Lumped Resistors; Satellite Communication;

Abstract

In this paper, a wideband metamaterial absorber (MMA) is proposed based on a resistively loaded square ring resonator. The proposed MMA consists of surface mounted 420 Ω lumped resistors and is designed on a FR-4 substrate. The proposed structure achieved over 90% absorption across a broad frequency range from 23.5 GHz to 28.65 GHz, with a peak absorption of 99.04% at 27.98 GHz having a Shielding effectiveness (SE) of 37.73 dB. The proposed meta-surface absorber shows polarization insensitive characteristics and upholds high absorption across a variety of incident angles. The absorption results achieved by CST studio suite, is further verified using HFSS software and the results are almost identical. The equivalent circuit model designed by ADS software to check the results and was found closely matched. The proposed design has undergone various simulations such as surface current analysis to check the absorption performance. In addition, Substrate thickness and area are also analyzed using parametric analysis to identify the optimal result. Moreover, the effect of various lumped resistors is also analyzed to understand the absorption mechanism. The proposed absorber covers key parts of the K-band, making the design suitable for satellite and 5G communication systems.

1. Introduction

The rapid development of wireless communication systems has led to a growing demand for competent and compact devices capable of limiting electromagnetic interference and enhancing signal strength. In high frequency applications such as satellite and 5G communications, the necessity of effective EM wave absorption has become a critical requirement. Conventional absorber materials often face limitations like narrow bandwidth, bulkiness, and sensitive to polarization and

[*]Corresponding author's E-mail address: nipun.murad@iubat.edu
Article received: June 2025 Revised and accepted: December 2025 Published: December 2025

incident angles. To find optimal solutions researchers have focused on metamaterial absorbers (MMAs), laboratory-engineered materials that possess unique electromagnetic characteristics not generally found in naturally occurring materials. Their ability to manipulate wave propagation, leads to great applications such as cloaking, superlensing, antennas, sensors, EM shielding and absorbers (Nipun *et al.*, 2025).

Several near-unity perfect absorber designs have been proposed by many researchers with different geometrical structures and patterns to achieve targeted performances. These include circular rings, square loops, split rings or cross shaped resonators with both symmetric and asymmetric structures with narrow or broad bands (Huang *et al.*, 2019), (Amiri *et al.*, 2020). In recent years, researchers have also explored designs that are not sensitive to polarization or angle of incidence, which are vital virtues for practical applications. The absorbers that have a simple and single-layer structure are more desirable than complex designs due to their fabrication complexity. For example, Hossain et al. developed a four-band metamaterial absorber that achieved almost perfect absorption, reaching up to 99.99%, making it well suited for EMI shielding applications (Hossain *et al.*, 2022; Kabir *et al.*, 2024). In contrast, many other designs that offer high absorption often face the drawback of limited bandwidth. A clear example is the work by (Nguyen *et al.*, 2018), whose structure, although polarization insensitive and capable of achieving peak absorption at 10 GHz, exhibited a narrow operational bandwidth of less than 0.5 GHz. To overcome this issue scientists have explored wideband approaches. For example, (Sun *et al.*, 2012) presented a broadband MMA using resistive layers and multiple resonator layers to maintain over 90% absorption throughout 8 to 18 GHz. At even higher frequencies, (Zhang *et al.*, 2020) proposed a wideband MMA for optical windows with absorption between 8-18 THz using multiple graphene layers for shielding applications. Also, (Nipun *et al.*, 2024) proposed a metamaterial absorber (MMA) optimized for dual-band absorption at 3.5 GHz and 13 GHz with peak absorption rates of 92.7% and 99.99%, respectively. The MMA, distinguished by polarization and incident angle insensitivity up to 60°, shows potential for applications in wireless communication and microwave sensing systems. From the above discussion the constant progress of MMA technology is in response to the challenges faced in creating compact and efficient electromagnetic systems.

In the presented work, a wideband absorber is proposed based on a resistively loaded square-circular hybrid resonator geometry. The absorber is designed on an inexpensive FR-4 substrate, a material commonly used in high-frequency circuit applications. It achieves more than 90% absorption across a wide frequency band from 23.5 to 28.65 GHz, with a peak value of 99.04% at 27.98 GHz. The structure is polarization insensitive and maintains consistent performance under different incident angles. To evaluate its stability and adaptability, several parametric studies were carried out, including analyses of surface current, substrate dimensions, and the effect of varying resistor values. The resulting operational bandwidth lies within the K-band, covering key frequency ranges of interest for emerging 5G networks

(24–24.25 GHz) and satellite uplink systems (27.5–28.35 GHz). The proposed design stands out from existing approaches by employing a hybrid square–circular resonator with optimized resistor loading, enabling wideband and polarization-insensitive absorption in a compact single-layer form, which is not demonstrated in the cited works. The proposed design delivers broadband, polarization-insensitive absorption and remains stable for incident angles up to 60°. With a compact footprint of 6 × 6 mm², its simple structure allows for low-cost fabrication. Simulations carried out in both CST and HFSS confirm the reliability of the results, while parametric and field analyses demonstrate strong magnetic resonance and effective impedance matching. These characteristics make the absorber a promising candidate for EMI shielding and modern communication applications.

2. Design of Proposed Unit-Cell

The essence of the proposed metamaterial absorber (MMA) is its carefully engineered unit-cell design, which enables strong absorption over a broad frequency range while remaining insensitive to both polarization and incident angle. The unit-cell configuration is composed of three essential layers: the top resonator layer, the middle dielectric substrate, and the bottom ground plane. The top layer consists of a square–circular hybrid resonator, which is loaded with four surface-mounted 420 Ω lumped resistors. These resistors are symmetrically positioned across the resonator's crosswise arms, contributing significantly to the electromagnetic performance by introducing controlled loss and impedance matching. Figure 1(a) illustrates the top view of the proposed unit-cell geometry, while Figure 1(b) shows the simulation setup used for full-wave electromagnetic analysis in CST Microwave Studio. The simulations were performed in CST Microwave Studio-2019 using a frequency-domain solver. Electric boundary conditions were applied along the X-axis, magnetic boundary conditions along the Y-axis, and open (add space) boundaries were set along the Z-axis to allow wave propagation. Waveguide ports were used to excite the structure for both TE and TM polarizations under normal and oblique incidences. A hexahedral mesh with adaptive refinement was applied, with denser meshing around the resonator edges and lumped resistors to capture fine electromagnetic details. The solver was configured with an energy residual convergence criterion to ensure numerical stability and accuracy. These settings were carefully chosen to balance computational efficiency with reliable and precise simulation outcomes. The geometric and material parameters of the unit cell are listed in Table 1. The resonator is implemented on an FR-4 substrate, which is widely available, inexpensive, and well known for its mechanical stability and suitability for high-frequency circuit applications. FR-4 has a relative permittivity (εr) of 4.3 and a loss tangent ($\tan \delta$) of 0.02, which moderately affect dielectric losses but still provide good performance at millimeter-wave frequencies.

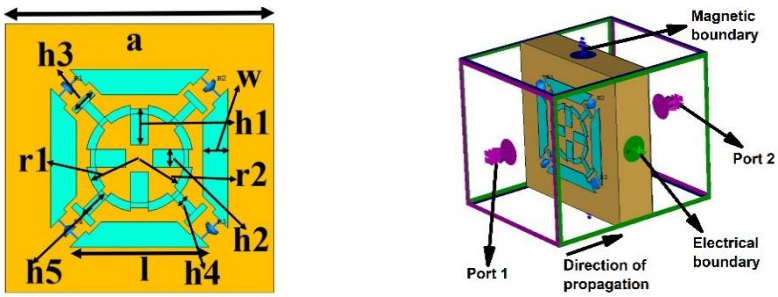

(a) (b)

Figure 1: (a) Top view of the proposed unit-cell structure showing the hybrid square–circular resonator loaded with four lumped 420 Ω resistors. (b) Simulation setup in CST Microwave Studio, illustrating the applied boundary conditions (electric along X, magnetic along Y, and open along Z) and Floquet port excitation used for normal and oblique incidence analysis.

Table 1: Geometric parameters and dimensional definitions of the proposed unit-cell structure optimized for wideband absorption within the K-band frequency range. The geometric parameters are defined as follows:

a – unit cell dimension; l – length of resonator arm; w – width of copper strip; t_s – substrate thickness; r_1 – inner circular radius; r_2 – outer circular radius; h_1–h_5 – layer thickness parameters corresponding to dielectric, copper, and spacing layers used in simulation and fabrication.

Parameters	**a**	**l**	**w**	**ts**	**r1**	**r2**	**h1**	**h2**	**h3**	**h4**	**h5**
Dimension (mm)	6	3.12	0.8	1.6	1.2	1	0.8	0.4	0.15	0.45	0.45

Both the resonator and the ground plane are fabricated using copper because of its high electrical conductivity ($\sigma = 5.8 \times 10^8$ S/m) and very low magnetic permeability ($\mu \approx 1$). The top resonator layer is designed to minimize reflection by matching its impedance to that of free space, whereas the copper sheet at the back of the substrate acts as a shield, completely preventing wave transmission. Each copper layer has a thickness of 0.035 mm, which exceeds the skin depth within the operating frequency range. This ensures that the electromagnetic energy remains effectively confined inside the absorber structure. The unit cell measures 6 × 6 mm², offering a compact footprint compared to many conventional absorber configurations. The resonator geometry was carefully optimized to achieve a broad operating bandwidth and stable impedance matching. By integrating an inner circular ring with an outer square loop, the design combines the benefits of both shapes. This hybrid configuration strengthens electromagnetic coupling and introduces several resonant modes that overlap, ultimately producing a smooth and continuous absorption band. This compact and symmetric design not only

minimizes the fabrication complexity but also promotes angular stability and polarization insensitivity.

The top resonator layer of the absorber is designed to make the reflection as close to zero as possible, while the ground plate acts as the blocking mechanism for transmission, making propagation null; both layers have a thickness of 0.035 mm. The skin depth of the incident EM wave can be calculated using the following equation (Kabir *et al.*, 2024):

$$\delta = \frac{2}{\sqrt{\omega\mu\sigma}} \quad (1)$$

where δ represents the skin depth, ω is the angular frequency, μ is the magnetic permeability, and σ is the electrical conductivity of copper.

Copper, a having permeability of $\mu = 1$ and a high conductivity of $\sigma = 5.8 \times 10^8$ S/m, has a blocking plate thickness greater than the calculated skin depth, thereby completely preventing propagation. In the meantime, the resonator patch is designed in such a that it matches the resonator's impedance with the free-space impedance, resulting in lower reflection and thus near-perfect absorption, as expressed by the following equation (Nipun *et al.*, 2025):

$$A = 1 - R - T \quad (2)$$

where A is the absorption, R is the reflection coefficient, and T is the transmission coefficient. Since the absorber includes a copper backplane, the transmission is effectively zero ($T = 0$), therefore the equation simplifies to:

$$A = 1 - R \quad (3)$$

The absorber design was simulated using CST Microwave Studio under unit-cell boundary conditions and Floquet ports to mimic infinite periodic arrays. The structure was analyzed using normal and oblique incidence of electromagnetic waves with both TE (transverse electric) and TM (transverse magnetic) polarizations. The impedance profile, surface current distribution, and H-field behavior were examined to validate the design's absorption mechanism. The performance was also verified by simulating the exact same structure in ANSYS HFSS, a finite element-based software, ensuring consistency and reliability of the results.

3. Result Analysis

To verify the performance of the discussed absorber, various analyses have been carried out. Figure 2(a) shows the magnitude curves for reflection, transmission and absorption. The absorber shows absorption levels more than 90% from 23.5 GHz to 28.65 GHz with a highest absorption of 99.04% at 27.98 GHz.

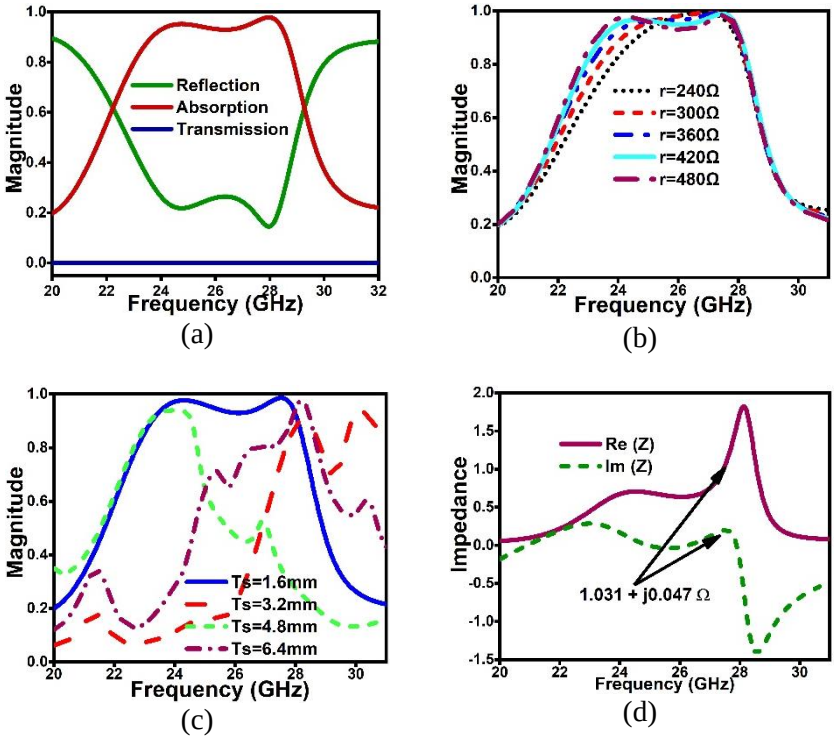

Figure 2: (a) Simulated absorption, reflection, and transmission spectra of the proposed absorber, showing more than 90 % absorption from 23.5 GHz to 28.65 GHz and a peak absorption of 99.04 % at 27.98 GHz. (b) Effect of varying lumped resistor values, highlighting 420 Ω as the optimal choice for wideband response. (c) Influence of substrate thickness, with 1.6 mm giving the best impedance match. (d) illustrates the normalized impedance of the proposed MMA, which is found to be approximately (1.031 + j0.047) at the target frequency. This value is close to unity, indicating an excellent impedance match with free space (377 Ω). It should be noted that the plotted quantity is normalized impedance, hence dimensionless.

Figure 2(b) shows the behavior of absorption results with different lumped resistors. This analysis is important as this element plays a key role in the reduction of the quality factor of the absorber. While a high Q-factor typically results in sharp and narrow resonance, lowering it broadens the absorption bandwidth, enabling wider frequency coverage and from the analysis it is clear that at r = 420 Ω, the optimal result is achieved. In Figure 2(c) the impact of the substrate thickness is shown, where the optimal result is achieved at a thickness of 1.6 mm. When the thickness increases it is observed that the absorption tends to degrade due to multiple reflections in the substrate, resulting in impedance mismatch. Figure 2(d) shows the impedance diagram of the proposed MMA and it is found that impedance is (1.031+j0.047) Ω at the desired frequency which is almost identical to the free-space impedance.

Figure 3 (a) shows the absorption characteristics over different substrate areas. The area is varied from 5.5 mm^2 to 6.5 mm^2 and from the analysis it is clear that the chosen area 6 mm^2 is the optimal one as a decrease in substrate area leads to insufficient surface current distribution resulting poor absorption, conversely, increasing the area makes the surface non-uniform for field and weaker surface current distribution, resulting in poor absorption. Figure 3 (b) and (c) show the surface current and H-field analysis at 27.98 GHz respectively. The power-loss density distribution shown in Figure 3 (d) highlights that most of the power dissipation occurs along the resonator edges and at the lumped resistor junctions, with very limited loss inside the dielectric substrate. This behavior confirms that the absorber operates mainly through resonant electromagnetic coupling rather than simple dielectric heating. Hence, despite the moderate loss of FR-4, the proposed design achieves stable and efficient broadband absorption.

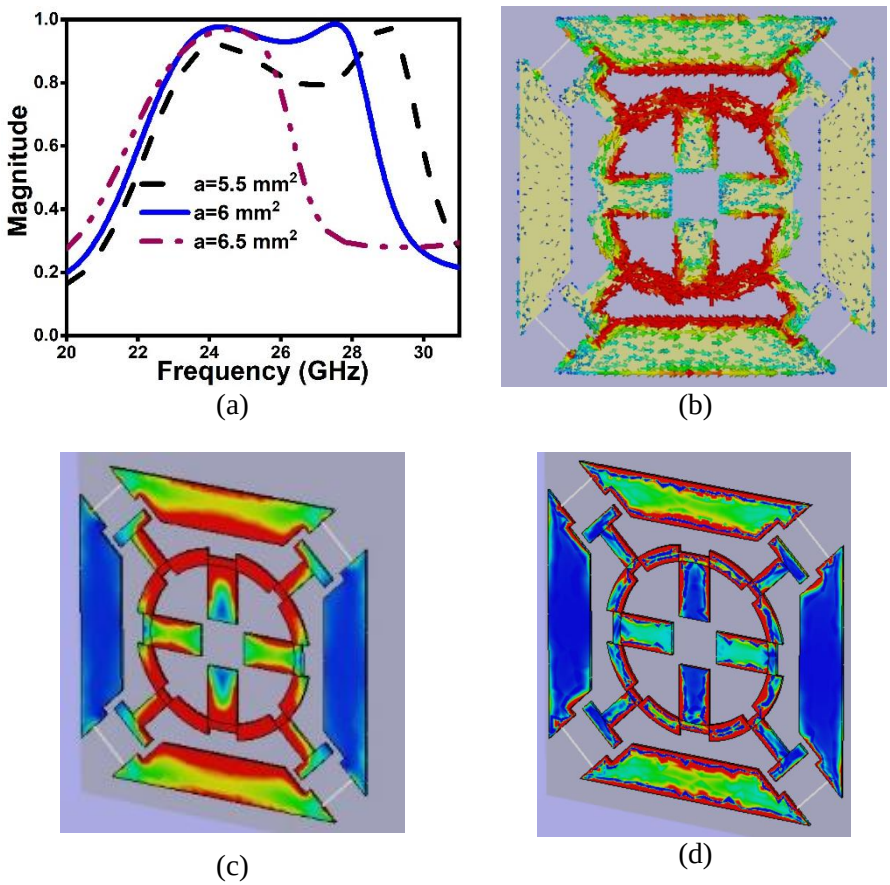

Figure 3: (a) Effect of substrate area variation on absorption performance, demonstrating that the chosen 6 mm^2 area provides optimal field uniformity and

surface current distribution. (b) Surface current distribution at 27.98 GHz, indicating strong localization along the resonator edges and junctions. (c) H-field distribution at 27.98 GHz, highlighting strong magnetic confinement at critical junction points. (d) Power-loss density distribution of the proposed absorber at 27.98 GHz, showing that losses are concentrated along the resonator edges and resistor junctions, confirming a resonance-dominated absorption mechanism.

The analysis of surface current distribution at peak absorption frequency of 27.98 GHz shows strong localization along the edges and junctions of the square circular resonator. The back side shows a strong current flow on the ground plate beneath the resonant region, indicating strong electromagnetic coupling. It is observed that the strong magnetic resonance arises from the reversed current direction between the resonator and the ground plane, which is also responsible for excellent impedance matching with free space. Also, H-field analysis shows the strong magnetic confinement at the edges of the junctions. In Figure 4 (a) and (b) the absorption characteristics with different oblique incident angles and polarizations are illustrated and the angular absorption map of the proposed absorber and demonstrate that the absorption of the proposed absorber at different incident and polarized angles remains very strong until it reaches 75°. The proposed design is also verified with another well-known software named HFSS as shown in Figure 4 (c) and (d). The outputs of the resonator have been analyzed and found to produce almost identical results.

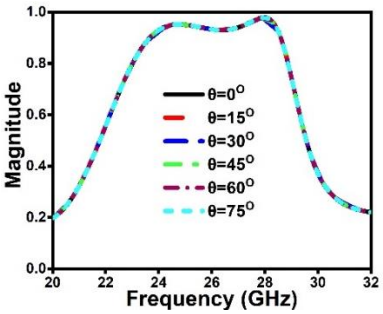

(a)

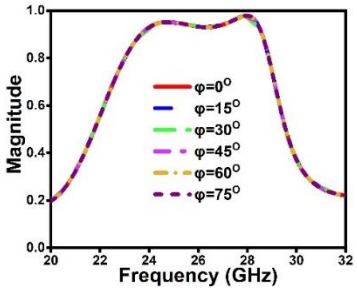

(b)

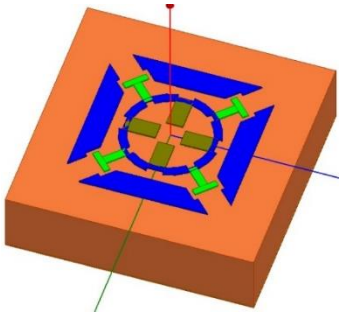
(c)

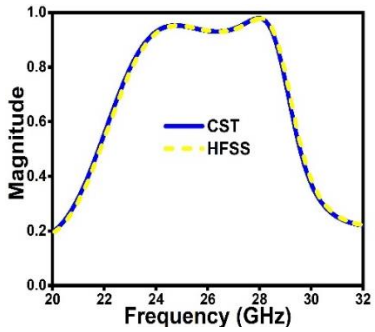

(d)

Figure 4: (a) Absorption performance for different polarizations, showing stable and polarization-independent behavior. (b) Absorption at various incident angles, maintaining over 90 % absorption up to 75°. (c) 3D model of the proposed MMA structure in HFSS for cross-validation. (d) Comparison of absorption spectra from CST and HFSS, demonstrating strong agreement between the two simulation platforms.

The equivalent circuit developed in ADS was constructed to emulate the electromagnetic response of the proposed metamaterial absorber (MMA) by combining several RLC resonant branches. The series resistor R_1(411 Ω) represents the surface-mounted 420 Ω resistors used in the actual design, introducing a controlled loss that helps suppress reflection and expand the absorption bandwidth. The branch composed of $L_3$and C_1(0.2825 nH and 0.139 pF) captures the high-frequency resonance associated with the circular portion of the structure, whereas the L_2–C_4–R_2branch (0.0232 nH, 1.06 pF, and 63.5 Ω) models the mid-frequency response. Similarly, the parallel branch L_4–C_2(0.07 nH and 0.907 pF) corresponds to the outer square loop, contributing to the lower-frequency portion of the absorption band. Together, these three resonant paths produce broadband absorption between 23.5 GHz and 28.65 GHz, showing close agreement with the CST simulation results. In the comparison graph, the ADS reflection curve (red) follows a similar profile to the CST data (black), with two distinct resonance dips that occur at nearly the same frequencies. Minor differences in amplitude and alignment are expected since ADS employs ideal lumped components, whereas CST performs full-wave electromagnetic modeling. Nonetheless, the ADS model successfully reproduces the essential absorption behavior of the proposed design, confirming the accuracy of the equivalent circuit representation.

To ensure the reliability of the equivalent circuit model, an iterative curve-fitting technique was applied in Keysight ADS. The initial RLC component values were estimated based on the resonant frequencies observed in the CST simulation and then refined through multiple optimization cycles to minimize the difference between simulated and modeled reflection coefficients. The fitting process aimed to align both the resonance positions and magnitudes of the reflection dips. The final optimized component values produced a correlation deviation of less than 3% across the operational band, indicating a strong match between the ADS and CST results. This close agreement confirms that the extracted circuit parameters effectively replicate the electromagnetic behavior of the proposed absorber, validating the use of the equivalent circuit approach for broadband absorption analysis. It is shown in Figure 5 (a) and (b).

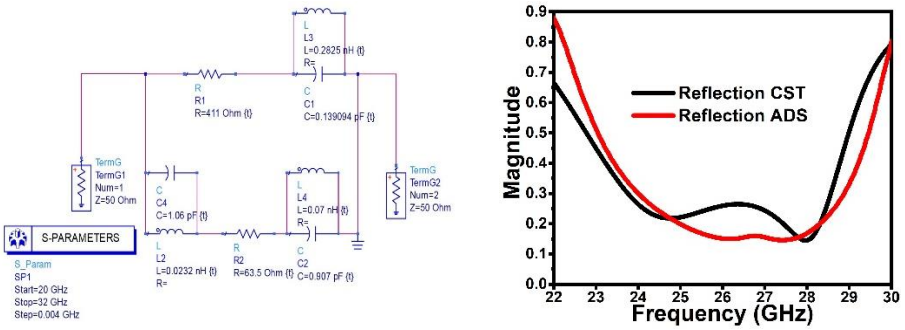

(a) (b)

Figure 5: (a) Equivalent RLC circuit model of the proposed absorber designed in ADS, representing multiple resonant paths that mimic the square–circular hybrid resonator. (b) Comparison between CST and ADS reflection responses, showing similar resonance dips and overall trend, confirming the accuracy of the equivalent circuit model.

To validate the use of FR-4 at K-band frequencies, the proposed absorber was simulated using three different substrates: FR-4 (εr = 4.3, tan δ = 0.02), Rogers RO4534 (εr = 3.55, tan δ = 0.0027), and Taconic (εr = 2.2, tan δ = 0.0009). The absorption responses, shown in Figure 6 (a), indicate that the FR-4-based design still maintains strong absorption performance despite its higher dielectric loss, demonstrating that the optimized hybrid resonator geometry and resistor loading effectively compensate for material limitations. To further examine material stability, a sensitivity analysis was conducted by varying the substrate's εr and tan δ by ±15 %. As presented in Figure 6(b), small shifts in the resonant peaks are observed, but the overall absorption level remains above 90 %, confirming the robustness of the absorber against material property variations commonly found in commercial FR-4.

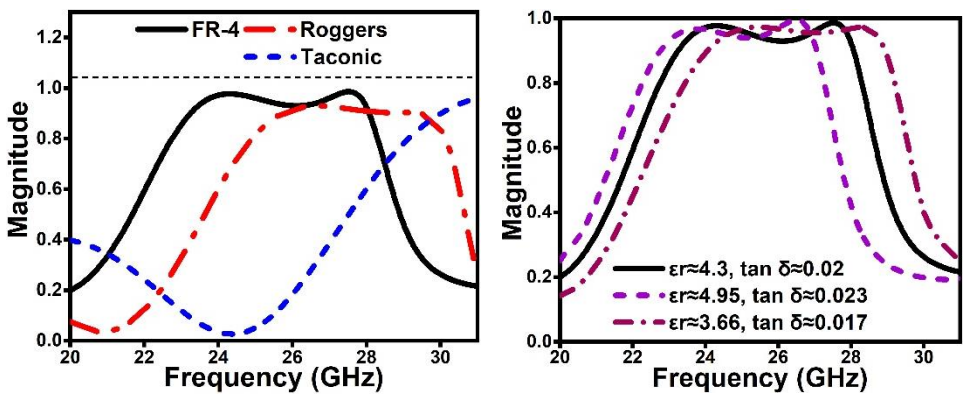

(a) (b)

Figure 6: (a) Comparison of absorption characteristics using different substrates (FR-4, Rogers, and Taconic). The FR-4-based design demonstrates strong absorption despite its higher dielectric loss, verifying the design's cost-effectiveness and adaptability. (b) Sensitivity analysis for ±15 % variations in εr and tan δ of FR-4. Only minor frequency shifts are observed, while absorption remains above 90 %, indicating high stability against material tolerance variations.

With the rapid growth of electronic devices, controlling unwanted electromagnetic (EM) radiation has become increasingly important. Metamaterial absorbers are particularly attractive for electromagnetic interference (EMI) shielding because their geometry and material properties can be tailored to achieve strong attenuation. Shielding effectiveness (SE) is a standard parameter used to quantify this capability, expressed in decibels (dB). It represents the combined effect of reflection, absorption, and multiple internal reflections in preventing EM waves from passing through the absorber. For practical designs, the contribution from internal reflections is usually negligible when the total SE exceeds 15 dB, allowing a simplified calculation using reflection (S_{11}) and transmission (S_{21}) coefficients. The total shielding effectiveness (SE), measured in decibels (dB), results from a combination of reflection loss (SER), absorption loss (SEA), and multiple internal reflections (SEM), as shown in Equation (4) (Bellal *et al.*, 2022):

$$SE(dB) = SE_R + SE_A + SE_M \quad (4)$$

where the reflection loss (SE_R) and absorption loss (SE_A) are calculated using the following expressions:

$$SE_R = 10log\left(\frac{1}{1-(S_{11})^2}\right) \quad (5)$$

$$SE_A = 10log\left(\frac{1-(S_{11})^2}{(S_{21})^2}\right) \quad (6)$$

In most practical cases, the contribution of internal reflections (SEM) is minimal, particularly when the overall SE is greater than 15 dB, so it can be ignored (Bellal *et al.*, 2022). This leads to a simplified expression for SE:

$$SE(dB) = 10log\left(\frac{1}{1-(S_{11})^2}\right) + 10log\left(\frac{1-(S_{11})^2}{(S_{21})^2}\right) \quad (7)$$

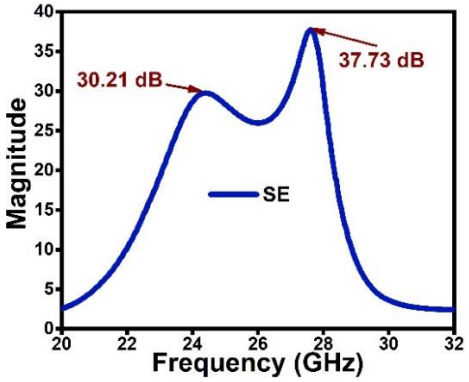

Figure 7: Simulated shielding effectiveness (SE) of the proposed absorber, showing peak values of 30.21 dB and 37.73 dB across the operating frequency band.

The SE of the proposed absorber was evaluated through simulation, as shown in Figure 7. The structure exhibits strong shielding performance across the operational band, reaching peak SE values of 30.21 dB and 37.73 dB at 24.32 GHz and 27.98 GHz respectively. These results confirm that the absorber provides effective EMI shielding within the target frequency range.

A comparison of the performance of the presented MMA is made with some other recent works. It is presented in Table 2, which assesses absorption bandwidth (BW), unit cell dimensions, and peak absorption. The comparison highlights the superiority of the proposed MMA, showing that it provides better performance within a more compact footprint.

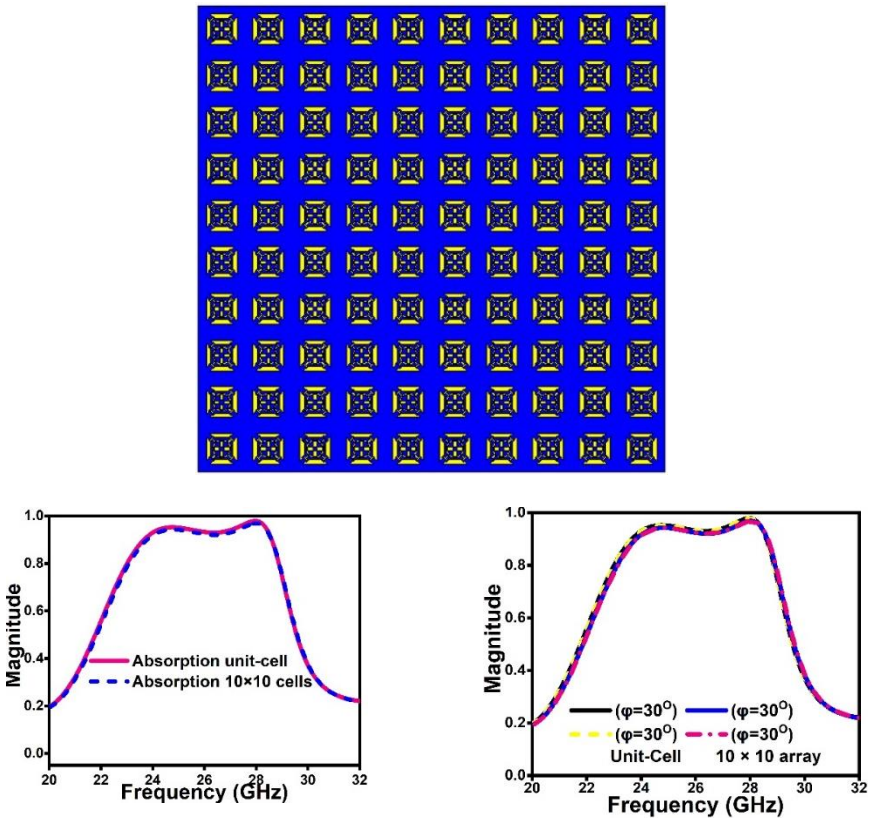

Figure 8: (a) Tow-dimensional model of the finite 10 × 10 array showing the overall arrangement of the unit cells. (b) Comparison of absorption performance between the infinite unit-cell model and the 10 × 10 array under normal incidence, demonstrating strong agreement between both configurations. (c) Comparison of absorption performance between the unit-cell model and the 10 × 10 array under oblique incidences (30° and 60°), confirming

that edge effects cause only minor deviations and the absorber maintains stable wideband behavior.

To verify that the absorption performance remains stable in a practical configuration, a finite absorber panel consisting of a 10 × 10 array of unit cells was simulated under both normal and oblique incidences. This analysis was carried out to examine the possible influence of edge coupling and truncation effects, which are often neglected in infinite periodic models. As illustrated in Figure 8(a), the overall arrangement of the 10 × 10 array follows the same geometry as the unit-cell model. Figure 8(b) compares the absorption responses of the infinite unit-cell and the finite array at normal incidence, showing almost identical broadband absorption with only a slight variation in magnitude. Similarly, Figure 8(c) presents the results for oblique incidences (30° and 60°), where the overall absorption profile remains above 90 % across the operating band. These results confirm that edge effects have minimal influence on the absorber's behavior and that the proposed design retains its wideband and polarization-independent characteristics even when implemented as a finite-sized surface.

Table 2: Comparison between the proposed absorber and recent related works in terms of absorption bandwidth, fractional bandwidth, unit-cell size in λ considering the first absorption frequency of the bandwidth, physical thickness, and peak absorption. The proposed design demonstrates superior bandwidth and absorption performance within a significantly more compact structure.

Absorption BW GHz at 90% absorption	**FBW (%)**	**Unit Cell size (mm^3)**	**Physical Thickness (mm)**	**Absorber type**	**Peak absorption (%)**	**Polarization insensitivity**	**Ref.**
5.5-7.58	31.8	0.26λ × 0.26λ × 0.03λ	1.6, 1	Double layer integrated with PIN diode	88.48	Up to 45°	(Shukoor *et al.*, 2023)
7.8-18	79.1	0.26λ × 0.26λ × 0.13λ	0.175, 3.5, 1.2	Multi-layer integrated with sheet resistors	93	Up to 45°	(Zhang *et al.*, 2020)
5.4-15.6	97.1	0.49λ × 0.49λ × 0.10λ	1.6, 14,	Double layer integrated	95	Up to 35°	(Qu *et al.*, 2018)

			0.762	with lumped resistors			
23.5-28.65	20	0.47λ × 0.47λ × 0.13λ	1.6	Single layer integrated with lumped resistors	99.04	Up to 75°	Proposed

Table 2 comparison reveals that while some existing absorbers have larger fractional bandwidths, they only work in lower frequency bands in which wider band absorption is relatively easier to attain. In contrast, the proposed structure has to work in the more difficult K-band frequency range in which losses in materials, fabrication errors, and size compactness further contribute to making wider band absorption harder to achieve. Even with lower FBWs, the proposed absorber is still better due to several capable and advantageous features such as the very high absorption of 99.04% at a very large incident angle of 75°, accomplished just in the simplest single-layer structure that doesn't use any active device and doesn't still require multi-layer absorption designs.

4. Conclusion

In this work, a compact and cost-effective wideband metamaterial absorber was designed and analyzed for K-band applications. By combining a square–circular hybrid resonator with lumped resistors, the structure achieved over 90 % absorption across 23.5–28.65 GHz, with a peak of 99.04 % at 27.98 GHz. The design maintained stable performance for both TE and TM polarizations under oblique incidence up to 60°, making it suitable for satellite and 5G communication systems. Beyond achieving strong numerical performance, the study highlights how simple geometric modifications, supported by careful impedance matching, can produce broadband absorption using a single-layer FR-4 substrate. This approach offers a practical pathway toward low-cost, easily manufacturable absorbers for real-world electromagnetic shielding. Since the proposed structure is based on a metallic microwave metamaterial topology on an FR-4 substrate, optical transparency is not applicable, as such materials are inherently opaque to visible wavelengths. Although the current work focuses on simulation-based analysis, the design was rigorously cross-verified using CST, HFSS, and ADS to ensure accuracy and reliability. Future work will focus on prototyping and experimental validation to further confirm the absorber’s performance, as well as exploring scaling for other frequency bands and multi-functional capabilities.

Acknowledgement

The authors would like to thank Miyan Research Institute, International University of Business Agriculture and Technology, Dhaka 1230, Bangladesh, for their helpful assistance.

Conflict of interest

The authors affirm that there are no conflicts of interest associated with the publication of this work. They have followed ethical guidelines and addressed various issues; including plagiarism, informed consent, misconduct, data fabrication and/or falsification, double publication and and/or submission, and redundancy. The authors have thoroughly observed and complied with ethical standards throughout the research and writing process.

Data availability

On request data might be available.

Ethical Approval

This research did not involve human participants, animals, or sensitive data; therefore, ethical approval was not required.

References

Amiri, M., Tofigh, F., Shariati, N., Lipman, J., & Abolhasan, M. (2020). Review on metamaterial perfect absorbers and their applications to IoT. *IEEE Internet of Things Journal, 8(6),* 4105-4131.

Hossain, I., Islam, M. T., Samsuzzaman, M., Moniruzzaman, M., Sahar, N. B. M., Almalki, S. H., ... & Islam, M. S. (2022). Polarization insensitive split square ring resonator based epsilon-negative and near zero refractive index metamaterial for S, C, and X frequency bands satellite and radar communications. *Scientific Reports, 12(1),* 9294.

KabirNipun, M. M., Islam, M. J., Moniruzzaman, M., Bashar, M. A., Nondi, R. K., & Al-Bawri, S. S. (2024, December). A Triple Band Compact Metamaterial Absorber for Ka-Band Satellite and Radar Applications. In 2024 6th *International Conference on Sustainable Technologies for Industry 5.0 (STI)* (pp. 1-4). IEEE.

Huang, C., Zhang, J., Cheng, Q., & Cui, T. (2019, December). Multi-band tunable asymmetric transmission of linearly polarized electromagnetic waves achieved by active chiral metamaterial. *In 2019 Photonics & Electromagnetics Research Symposium-Fall (PIERS-Fall)* (pp. 325-331). IEEE.

Nguyen, T. T., & Lim, S. (2018). Angle-and polarization-insensitive broadband metamaterial absorber using resistive fan-shaped resonators. *Applied Physics Letters, 112*(2).

Nipun, M. M. K., Islam, M. J., & Moniruzzaman, M. (2025). A triple-band metamaterial absorber for gas sensing and refractive index detection through enhanced FOM and Q-factor performance in the THz regime. *Results in Optics, 21,* 100822.

Nipun, M. M. K., Islam, M. J., & Moniruzzaman, M. (2025). An Optimal Ultra-Thin Broadband Polarization-Independent Metamaterial Absorber for Visible and Infrared Spectrum Applications. *Electronics Letters, 61(1),* e70314.

Nipun, M. M. K., Islam, M. J., Moniruzzaman, M., Jusoh, M., Vettikalladi, H., Almuhlafi, A. M., ... & Al-Bawri, S. S. (2024). Interconnected Circular Ring Resonator based Single Negative Perfect Metamaterial Absorber for Wireless Communication Systems. *Optical and Quantum Electronics, 56(6),* 1053.

Qu, M., Sun, S., Deng, L., & Li, S. (2018). Design of a frequency-selective rasorber based on notch structure. *IEEE Access, 7,* 3704-3711.

Shukoor, M. A., & Dey, S. (2023). Wideband reconfigurable multifunctional absorber/reflector with bandpass/bandstop filtering and band-notch absorption for RCS and EMI shielding. IEEE Transactions on Electromagnetic *Compatibility, 66(1),* 153-160.

Sun, L., Cheng, H., Zhou, Y., & Wang, J. (2012). Broadband metamaterial absorber based on coupling resistive frequency selective surface. *Optics express, 20(4),* 4675-4680.

Zhang, Y., Dong, H., Mou, N., Chen, L., Li, R., & Zhang, L. (2020). High-performance broadband electromagnetic interference shielding optical window based on a metamaterial absorber. *Optics Express, 28(18),* 26836-26849.

Hossain, M. B., Faruque, M. R. I., Islam, M. T., Singh, M., & Jusoh, M. (2022). Triple band microwave metamaterial absorber based on double E-shaped symmetric split ring resonators for EMI shielding and stealth applications. *Journal of Materials Research and Technology, 18,* 1653-1668.